Experimental and theoretical comparison of ^{27}Al,^{7}Li, and ^{13}C magic-angle-spinning NMR spectra for metal-atom clusters with rotational symmetry in their unit cells

M. C. Palenik, C. A. Klug, M. W. Conroy, S. A. Fischer, D. Gunlycke, B. I. Dunlap, L. Stevens, P. Zavalij, and B. Eichhorn

Experimental and theoretical comparison of ^{27}Al, ^{7}Li, and ^{13}C magic-angle-spinning NMR spectra for metal-atom clusters with rotational symmetry in their unit cells

M. C. Palenik[a]* and C. A. Klug[a], M. W. Conroy[a], S. A. Fischer[a], D. Gunlycke[a], B. I. Dunlap[b]
Chemistry Division, Naval Research Laboratory, Washington, DC 20375, USA[a], Volunteer emeritus[b]

L. Stevens, P. Zavalij, and B. Eichhorn
Department of Chemistry and Biochemistry, University of Maryland, College Park, MD 20742, USA

Some metal complexes and clusters can crystalize into structures with high rotational symmetry in the asymmetric unit cell. For such systems, magic angle-spinning NMR is particularly appropriate for detecting these symmetries and the corresponding local atomic coordination. In this work, we study three related metal-atom clusters: LiAlH$_4$, LiAlPh$_4$, and the [Li(Bu$_2$O)$_3$][Li$_4$Al$_5$Ph$_{12}$] cluster, which we recently synthesized. For the two trivalent aluminum species, we compare NMR parameters obtained from experiment and density-functional theory (DFT) calculations, including chemical shielding, nuclear quadrupolar interactions, and the Al-C1 J-coupling constant of LiAlPh$_4$. The NMR parameters were extracted from measurements at two very different magnetic fields, 11.7 T and 2.35 T. The low field measurements were crucial for both the direct spectra observation of the Al-C1 J-coupling and the precise determination of the Al quadrupolar interaction in LiAlPh$_4$. We also present DFT-derived NMR parameters for the larger [Li(Bu$_2$O)$_3$][Li$_4$Al$_5$Ph$_{12}$] cluster.

I. INTRODUCTION

Metal formation and dissolution processes often occur via metal-atom cluster intermediates, whose chemical properties and reactivities vary considerably from the bulk metallic phase. Such clusters are interesting not only because of their unusual structures, reactivities, and fundamental role they play in in chemistry [1], but because aluminum cluster intermediates containing atoms in a reduced oxidation state (between 0 and 3) show potential for use as energetic materials.

Low oxidation state aluminum clusters can be synthesized via a salt metathesis and disproportionation reaction involving Al(I) halide precursors and anionic organic ligands. This process can result in discrete metal-atom clusters containing both metal-metal and metal-ligand bonds, and may futhermore produce metalloid clusters,which are characterized by a greater number of metal-metal bonds than metal-ligand bonds. An example of a non-metalloid, metal-atom cluster that can be produced by disproportionation is Al$_4$Cp$^*_4$, which has four aluminum atoms arranged in a tetrahedron, each of which is connected by five bonds to a pentamethylcyclopentadiene ligand. On the other hand, Al$_{50}$CP$^*_{12}$, which has two concentric, approximately icosahedral aluminum shells surrounded by twelve pentamethylcyclopentadiene ligands, is metalloid in nature.

While Al$_{50}$Cp$^*_{12}$ has been synthesized [2] and characterized via nuclear magnetic resonance (NMR) [3], it has yet to be independently reproduced. This is largely because the disproportionation pathway is highly complex, and dependent on numerous factors such as reaction solvent, temperature, and identity of organic ligands. These combined factors occlude the ability to rationally design

syntheses to isolate Al clusters of a specific nuclearity. Additionally, numerous reported Al clusters face issues with low yield, poor reproducibility, or instability, limiting studies and characterizations.

Due to the quadrupolar nature of the 27-Al nucleus, solution-based NMR typically gives rise to broad signals with low spectral resolution, an issue partially mitigated by magic angle spinning (MAS) solid-state NMR analyses. Thorough investigations of the properties of highly reproducible Al clusters obtained from disproportionation pathways will provide crucial insight into potential similarities of stable clusters, including the role of ligands and Al oxidation states. These studies may aid in future ability to rationally design experiments and ligands to stabilize clusters of specific nuclearity.

Utilizing the disproportionation of Al(I)Br solutions, we have developed syntheses to reliably isolate two aluminum-containing species in the solid state: [Li(Bu$_2$O)$_3$][Li$_4$Al$_5$Ph$_{12}$], a mixed-valent, five-atom aluminum cluster, and LiAlPh$_4$, a high-valence species containing Al^{3+}. While the [Li$_4$Al$_5$Ph$_{12}$]$^{1-}$ cluster anion is non-metalloid in nature, it is highly reproducible across a variety of reaction conditions, an aspect that we attempt to understand through NMR and density functional theory (DFT) investigations. While LiAlPh$_4$ has been reported as a molecular species [4], the crystallographic modification studied here, isolated from Al(I)Br disproportionation reactions, is a highly symmetric polymer. Study of LiAlPh$_4$ establishes groundwork that may be applied to larger systems. Additionally, commerically available LiAlH$_4$ [5] was studied as a simplified analogue of LiAlPh$_4$, providing metrics to compare two trivalent Al atoms in similar coordination environments.

LiAlH$_4$ crystallizes in a monoclinic lattice, space group $P2_1/c$. Figure. 1 depicts the unit cell of LiAlH$_4$ (left), and an isolated [AlH$_4$]$^-$ anion, which exhibits a central Al^{3+} bound to four hydrogens in a nearly tetrahedral ar-
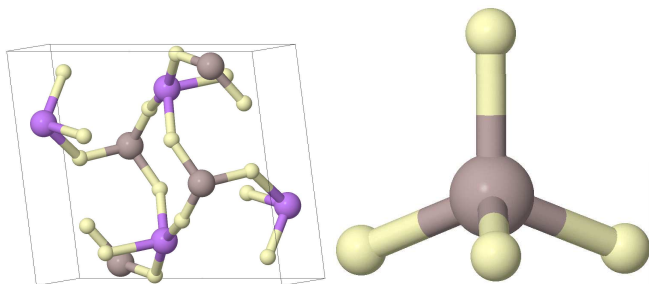
FIG. 1. (Left) The full translational unit cell of LiAlH$_4$ (Right) Single AlH$_4$ anion.

rangement. The unit cell can be split into two halves related by inversion. Each half is composed of two formula units related by a two-fold rotation. Thus all the Li or the Al atoms are equivalent by symmetry. These symmetries do not constrain the arrangement of hydrogen atoms around the aluminum atom, but the angles deviate only slightly from tetrahedral.

LiAlPh$_4$ crystallizes in the tetragonal space group $P\bar{4}2_1/c$. An isolated molecule of LiAlPh$_4$ consists of a central Al^{3+} atom bound in an eta^1 fashion to four phenyl ligands in S$_4$ symmetry. The asymmetric unit contains one Li, one Al, and one phenyl ring, which generate all other atoms in the unit cell by symmetry operations. In isolation, AlH$_4$ is much more symmetric than AlPh$_4$, yet the unit cell of LiAlPh$_4$ is more symmetric then that of LiAlH$_4$, containing eight rather than four symmetry operations. The AlPh$_4$ anion crystalizes with a lithium cation into a tetragonal lattice having $P\bar{4}2_1/c$ symmetry, while tetrahedral AlH$_4$ crystalizes into a monoclinic lattice in the $P2_1/c$ space group.

Figure 2 depicts the full, translational unit cells of LiAlPh$_4$, on the left, and [Li(Bu$_2$O)$_3$][Li$_4$Al$_5$Ph$_{12}$] on the right, and the cell parameters are given in Table I. Individual formula units of these compounds are shown in Fig. 3. Two formula units of LiAlPh$_4$ are contained in its unit cell, with one split between four edges, and the [Li(Bu$_2$O)$_3$][Li$_4$Al$_5$Ph$_{12}$] unit cell contains four formula unit. Not only is the number of formula units greater in the [Li(Bu$_2$O)$_3$][Li$_4$Al$_5$Ph$_{12}$] unit cell, but each [Li$_4$Al$_5$Ph$_{12}$]$^-$ anion is much larger than each LiAlPh$_4$ anion. The high number of rotational symmetry in these unit cells could indicate that It is possible for disproportionation processes to favor rotational symmetry in clusters and the asymmetric unit cells of crystals because the same molecular unit can be formed from chemical reactions that occur in multiple orientations.

While ^{27}Al NMR of LiAlH$_4$ has been observed in Magic Angle Spinning (MAS) experiments previously [6, 7], we have repeated these measurements in addition to performing ^{27}Al and ^{13}C MAS NMR measurements for LiAlPh$_4$. NMR signals are sensitive to the motion of electrons about individual nuclei and thus can distinguish between the local environments of nuclei in different compounds and different sites within a compound,
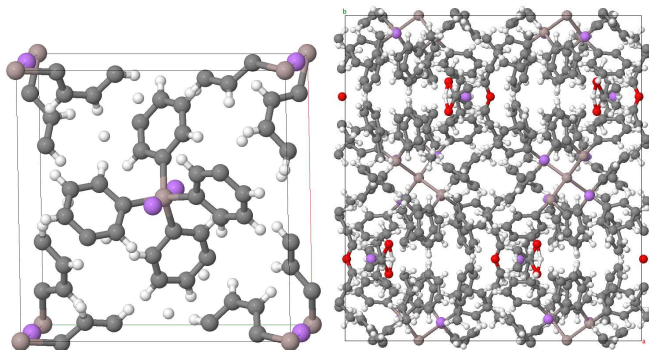

FIG. 2. (Left) The full translational unit cell of LiAlPh$_4$ (Right) The full translational unit cell of [Li(Bu$_2$O)$_3$][Li$_4$Al$_5$Ph$_{12}$]
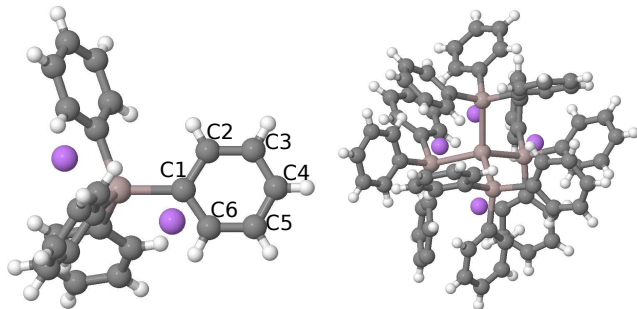

FIG. 3. (Left) A single LiAlPh$_4$ cluster from surrounded by two Li$^+$ cations (right) A single Al$_5$Ph$_{12}$ cluster surrounded by four Li$^+$ cations

which makes it a valuable tool for structural investigation. The chemical specificity of the NMR measurements arises from the field-induced electronic current perturbing the magnetic field differently at each nucleus. The induced current creates an opposing magnetic field that shields the nucleus from the external magnetic field. Prediction of the chemical shielding tensor, $\overleftrightarrow{\sigma}$, requires calculation of the induced current and its associated magnetic field. Due to recent advances in density-functional perturbation theory that allow a periodic calculation for a crystal to be perturbed by an applied electromagnetic field [8, 9], many crystalline DFT codes are now able to compute field induced effects on crystals. We use Quantum Espresso [10] to calculate the chemical shielding of ^{27}Al, ^{13}C, and ^{7}Li isotopes within the compounds of interest. Relative chemical shieldings can be compared to experimental NMR isotropic chemical shifts.

Additionally, non-spherical nuclei, $i.e.$, those with spin $> \frac{1}{2}$, have a non-zero quadrupole moment that interacts with the electric field gradient of the surrounding electrons and contributes to the difference in energy levels between different nuclear spin states. The spherical ^{13}C nucleus has a spin of $\frac{1}{2}$. The quadrupolar isotopes in our study are the ^{27}Al nucleus, with a spin of $\frac{5}{2}$ and Q = 0.149 barn, and the ^{7}Li nucleus, with a spin of $\frac{3}{2}$

TABLE I. Symmetry and structural information for LiAlH$_4$ and LiAlPh$_4$. Data are for the full translational unit cells. The crystal structure of LiAlH$_4$ is reported in Ref. [5].

Crystal	Bravais lattice	Space group	Atoms	Volume (Å^3)	a(Å)	b(Å)	c(Å)	β
LiAlH$_4$	monoclinic	$P2_1/c$	24	275.180	4.825	7.804	7.8974	112.268°
LiAlPh$_4$	tetragonal	$P\bar{4}2_1/c$	92	896.486	11.9520	11.9520	6.2757	–
[Li(Bu$_2$O)$_3$][Li$_4$Al$_5$Ph$_{12}$]	Orthorhombic	$P2/n\ 2_1/n\ 2/a$	1012	9773.978	23.105	25.384	16.665	–

and Q $= -0.0406$ barn, with the negative sign indicating an oblate, rather than prolate, spheriodal nucleus. The quadrupole moment is primarily a property of the nucleus alone, and measured values are available in the literature for common nuclei [11]. On the other hand, the electric field surrounding the nucleus depends strongly on the local environment of the isotope. The quadrupolar interaction can be predicted by calculating the electric field gradient tensor at the nucleus and coupling that to arbitrarily oriented quadrupole moment of the nucleus. Crystalline DFT methods have historically calculated the electric field gradient tensor surrounding the nuclei. The quadrupolar interaction is characterized by coupling constant C$_Q$ = eQ V$_{ZZ}/h$ and asymmetry parameter, $\eta = (V_{XX} - V_{YY})/V_{ZZ}$, where V$_{XX}$, V$_{YY}$, and V$_{ZZ}$ are the principal components of the electric field gradient tensor (ordered by convention, $|V_{ZZ}| \geq |V_{YY}| \geq |V_{XX}|$), e is the fundamental charge, and h is Planck's constant.

NMR crystallography and DFT are ideal tools for probing these symmetries, and we have used a combination of these techniques to study LiAlH$_4$, LiAlPh$_4$, and [Li(Bu$_2$O)$_3$][Li$_4$Al$_5$Ph$_{12}$]. Although we were unable to obtain experimental NMR for the third cluster, the use of both techniques in conjunction where possible provides insight into cluster chemistry in general and the constraints of unit-cell symmetry on the NMR spectra in particular.

II. SYNTHESIS OF [LI(BU$_2$O)$_3$][LI$_4$AL$_5$PH$_{12}$]

The low-valent method of producing aluminum clusters, pioneered by Schnöckel, first involves a comproportionation reaction between Al(s) and HX(g) at high temperature and low pressure to produce Al(I)X solutions. These metastable precursors, which contain aluminum in a pre-reduced state, undergo disproportionation via the reaction $3AlX \rightarrow 2Al + AlX_3$. By introducing an anionic organic reagent, R$^-$, during the disproportionation process, in a form such as LiR, a salt metathesis reaction drives the formation of low-valent aluminum clusters of the form Al$_n$R$_m$.

To generate cocrystals of [Li(Bu$_2$O)$_3$][Li$_4$Al$_5$Ph$_{12}$] and Ph$_{12}$ and LiAlPh$_4$, a precursor solution containing Al(I)Br in a toluene / diethyl ether matrix was reacted with phenyllithium (LiC$_6$H$_5$) in dibutyl ether. The pheynl ligand was chosen because of its sigma donor properties and lack of reactive beta hydrogen atoms, attributes which have previously been noted to stabilize

clusters with low-valent Al atoms. Thestructures of both products were determined by single crystal X-ray diffraction. Unfortunately, we were not able to isolate sufficient quantities of the larger cluster for NMR measurements, which typically requires at least 10 mg of material.

III. THEORY

In this work, we use two DFT band-structure codes to calculate NMR parameters, Quantum Espresso (QE) [10] and CRYSTAL14 (CRYSTAL) [12]. Both codes use periodic boundary conditions for the electron wavefunctions. The same semi-local PBE functional [13], used to describe exchange and correlation effects, is available in both band-structure codes. Most NMR calculations on solids use that functional [14].

QE uses the planewave basis set and pseudopotentials, which is a particularly efficient approach because only a small subset of electrons are explicitly treated. On the other hand, symmetry is an important consideration in this work and can be fully exploited in the all-electron Gaussian basis set code CRYSTAL [15]. Recent work has shown that plane-wave pseudopotential calculations are becoming much more standardized [16], and therefore, we should expect considerable agreement between these two codes.

Although the primary difference between the codes is the basis set used to calculate the electron wavefunctions, there are many other differences as well. Only one of the codes (Approach 1) is able to calculate the chemical shieldings that can be used to predict chemical shifts. On the other hand, the other code (Approach 2), can use the hybrid B3LYP functional [17]. That functional contains an optimized amount of exact exchange and thus would be expected to give more accurate atomization energies (however atomization energies are not considered in this work). Gaussian09 [18] was used to obtain a J-coupling value.

A. Approach 1: Planewave basis with pseudopotentials

The open-source QE 5.4.0 code performs DFT calculations with a planewave basis to calculate the valence electron wavefunctions and pseudopotentials to approximate the effects of the core electrons. Of central importance for the NMR calculations is the reconstruc-

tion of the all-electron wavefunction from the pseudopotential wavefunction. In the gauge-including projector-augmented wave (GIPAW) method, that linear transformation explicitly includes the magnetic field in a way that ensures translational periodicity [14]. We chose the GIPAW Troullier-Martins norm-conserving potentials that were generated by D. Ceresoli: Al.pbe-tm-gipaw-dc.UPF; C.pbe-tm-new-gipaw-dc.UPF; Li.pbe-tm-gipaw-dc.UPF; H.pbe-tm-new-gipaw-dc.UPF that are available on a website [19].

Starting from the experimental crystal structures, two optimizations are possible. In the simplest, only the atomic coordinates were optimized with a fixed unit cell. In longer calculations, both the atomic coordinates and the lattice were optimized. All optimizations reported in this work preserve the experimental space group, and therefore use only the first type of optimization. For that, we used the following convergence criteria: the energy change between optimization steps was less than 10^{-5} Rydberg (Ry), or approximately 1.4 x 10^{-4} eV, and the maximum force on any atom was less than 10^{-4} Ry/Bohr (5 x 10^{-3} eV/Å). We also performed calculations with both tolerances reduced by an order of magnitude, and there were small differences in the calculated electric field-gradients and less difference in the shielding parameters. Test lattice optimization had a similar effect. The shielding parameters were essentially the same, but the quadrupolar NMR parameters showed variability within the range of that shown in the tables below. To reduce the parameter space involved in comparing experiment and theory, the X-ray lattice parameters were used to determine all NMR parameters reported in this work.

We chose the energy cutoff for the planewave basis set and k-point sampling in the unit cells based on convergence tests of the NMR parameters. The convergence tests included calculations with energy cutoffs ranging from 20 to 120 Ry (with fixed 2x2x2 k-point meshes) and k-point meshes of 1x1x1, 2x2x2, and 3x3x3 (with fixed energy cutoff of 80 Ry). Based on these tests, we chose an energy cutoff of 80 Ry (1088 eV) for all calculations reported in this work. We used a 2x2x2 k-point mesh (8 k-points); the maximum corresponding k-spacing for $LiAlH_4$ is about 0.1 Å^{-1} (smallest lattice vector a= 4.8174 Å) and for $LiAlPh_4$ is about 0.08 Å^{-1} (smallest lattice vector c= 6.2757 Å). Our calculations indicate the following convergence levels with respect to energy cutoff and k-points: chemical shieldings < 0.5 ppm, quadrupolar coupling constants < 2%, and asymmetry parameters < 10%.

B. Approach 2: Gaussian-type basis

We also used the commercial code, CRYSTAL14 [12], which performs DFT calculations using Gaussian-type basis functions for both core and valence electrons. This allows selection of and comparison between different Gaussian basis sets. The use of big Gaussian basis sets in

band-structure calculations is problematical because very diffuse functions have significant weights in multiple unit cells. Thus a cutoff must be used to remove such basis functions from the standard basis sets of quantum chemistry. A very good and well established quantum chemistry basis set is the Pople, triple-ζ 6-311G** basis set [20]. The corresponding m-6-311G(d) basis set was used for Al [21]. It is a modification (m-) of the corresponding Pople basis set that removes essentially all Gaussian exponents smaller than 0.12 in atomic units (a.u.). The full 6-311G** basis set was used for C and H. For Li the two most diffuse sp exponents were replaced with a single exponent of 0.12. This basis set is called 6-311 hereafter and was used by CRYSTAL14 to optimize the geometries of the two crystals with fixed, experimental unit-cell dimensions. Another basis set, pob-TZVP, is also triple-ζ. It is based on the newer TZVP-def2 molecular basis. The two atomic basis sets, before modification, are actually quite different. Except for Al, the tightest exponents are significantly tighter in TZVP-def2. Its modification, pob-TZVP (POB in the following) has a lower Gaussian exponent threshold of 0.1, compared to 0.12 for 6-311, but uses relatively more highly contracted cores and less contracted valence Gaussian basis functions [22]. Apart from Al, the number of of primitive and contracted functions is the same for both basis sets, if we take every combined sp 6-311 basis function to actually be four, one s and three p, functions. For Al the modified basis sets are very different. The primitive s basis of 6-311 has twelve functions, while that of POB has fourteen, but the POB contracted basis for Al has two fewer s functions and one fewer p function. There are clearly going to be differences, but we expect that comparison among the results using these two very good Gaussian basis sets in CRYSTAL calculations and the results of well converged QE calculations to indicate the level of agreement to be expected between experiment and theory for NMR spectra of this important class of materials.

Only the atomic coordinates were optimized; the experimental X-ray lattice constants were held fixed. For comparing relative energies, we used the default self-consistent-field convergence criterion for CRYSTAL that the energy change between cycles was less than 10^{-7} a.u. and the default optimization criteria: The root-mean square (RMS) of all gradients had to be less than 3.0 x 10^{-4} a.u., and the RMS incremental displacements had to be less than 1.2 x 10^{-3} a.u. As a first test, we computed the CRYSTAL 6-311 energy using the QE optimized geometry. This energy was 2x10^{-5} a.u. higher, consistent with the variational principle. The optimized structures using these very different methods are quite similar and suggest that both sets of calculations should be reliable within the PBE approximation of DFT. There is less agreement between the QE and CRYSTAL POB optimized structures. With the POB basis, the difference in energy between the QE geometry and the fully optimized geometry is 2x10^{-3} a.u. Thus these two geometries are further apart. Furthermore, the optimized

POB energy is 0.074 a.u. higher than the 6-311 energy, indicating, through the variational principle, a worse basis set. The Al C_Q values at the QE geometry are 3.91 and 3.89 MHz in the 6-311 and POB basis sets, respectively

In order to converge B3LYP calculations in any nearby geometry, the number of sampling points in the irreducible Brillouin zone had to be increased from eight to thirty by doubling the shrink parameters. Doubling the shrink parameters for PBE calculations had negligable effects, and this variation was only used for B3LYP calculations on LiAlH$_4$.

Consistent with our choice for QE calculations, we reduced the geometry optimization criteria by a factor of ten for our remaining CRYSTAL calculations. The root-mean square (RMS) of all gradients had to be less than 3.0×10^{-5} a.u., and the RMS incremental displacements had to be less than 1.2×10^{-4} a.u. Each of the Coulomb and exchange truncation tolerances for calculating bielectronic integrals were also decreased from their default values by one and two orders of magnitude, 10^{-8} and 10^{-16}, respectively. Our test calculations showed that further reduction in these tolerances had a relatively small effect on the predicted NMR parameters. The need to decrease tolerances in both approaches is indicative of the sensitivity of these calculations. In particular the energy converges much faster in these codes than do the NMR parameters. While the NMR parameters are not absolutely converged, any improvement that can be made to any one calculation is expected to be less than the difference between values of parameters calculated by the three methods that is seen in the tables below.

IV. EXPERIMENTAL: NUCLEAR MAGNETIC RESONANCE

Room temperature NMR spectra were obtained using a Varian NMR500 spectrometer. Two magnetic fields were used: 11.7 T and 2.35 T. The same 4 mm triple-resonance MAS NMR probe was used with both superconducting magnets and all samples were loaded into the 4 mm rotors under a dry nitrogen environment. The high field ^{27}Al and ^{7}Li NMR spectra were acquired using single-pulse excitation with small flip angle pulses whose lengths ranged from 0.5 to 1.2 μsec. For the low field ^{27}Al NMR spectrum, the long probe recovery necessitated using a rotor-synchronized spin echo with first and second pulse lengths of 2 μsec and 4 μsec respectively separated by 62.5 μsec. For both the high- and low-field ^{27}Al NMR spectra, continuous-wave proton decoupling of 100 kHz was used. The ^{13}C NMR spectra were acquired via cross-polarization from ^{1}H to ^{13}C with the matching fields set to 50 kHz and 100 kHz CW proton decoupling. Spinning speeds varied from 10 to 16 kHz. The ^{27}Al and ^{13}C chemical shifts, given by the parameter δ, are referenced to 0 ppm for 1M Al(H$_2$O)$_6^{3+}$ aqueous solution and TMS respectively. Spectral simulations were per-

TABLE II. Calculated solid-state NMR parameters for ^{27}Al and ^{7}Li in LiAlH$_4$. The first row for each nucleus are from a planewave pseudopotential Quantum Expresso calculation and the remaining are CRYSTAL14 calculations.

Nucleus	Method	C_Q MHz	η	σ (ppm)
^{27}Al	PBE QE	3.65	0.409	456.47
	PBE 6-311	3.84	0.358	-
	PBE POB	4.70	0.411	-
	B3LYP 6-311	4.10	0.386	-
	B3LYP POB	4.80	0.420	-
^{7}Li	PBE QE	-0.0506	0.311	90.22
	PBE 6-311	-0.0461	0.364	-
	PBE POB	-0.0357	0.526	-
	B3LYP 6-311	-0.0375	0.327	-
	B3LYP POB	-0.0328	0.813	-

formed using the SIMPSON program [23]. All relevant experimental spectra and their corresponding simulated spectra are shown in the supplemental information.

V. RESULTS AND DISCUSSION

A. LiAlH$_4$

The crystal structure was optimized using fixed, experimental lattice dimensions using both computer codes. The NMR parameters calculated for ^{27}Al and ^{7}Li within LiAlH$_4$ are shown in Table II. All theoretical NMR parameters are within twenty percent of the averages except for the unusually high B3LYP POB η value for ^{7}Li, which cannot be associated with the very small ^{7}Li C_Q magnitude, because the smallness of that value is due to the smallness of the Li nuclear quadrupole moment and not the electric-field gradients. There is a significant difference in the two Gaussian basis sets using B3LYP. The calculated ^{27}Al η values are between 0.358 and 0.420. The calculated ^{7}Li C_Q values are consistently small and negative. These results are unlikely to change significantly with paramenters input to either code. Experimental values obtained by us and from other works are given in Table III. Only the magnitude of C_Q is obtained experimentally, and thus the measured and computed values for ^{7}Li differ by a minus sign. Otherwise, the computed and experimental quadrupole couplings differ by between two and twenty percent, depending on method.

B. LiAlPh$_4$

The NMR parameters calculated for ^{27}Al and ^{7}Li within LiAlPh$_4$ are shown in Table IV. In contrast to the relatively simple unit cell of LiAlH$_4$, LiAlPh$_4$ has an unusual crystal structure that has rotational symmetry within the unit cell. In particular, the Li-Al bond in the latter crystal is along a two-fold symmetry axis. This

TABLE III. Experimental measurements of NMR parameters for LiAlH$_4$.

Source	Nucleus	$|C_Q|$ MHz	η	δ (ppm)
Kellberg, et al. [7]	^{27}Al	3.90 ± 0.05	0.30 ± 0.05	102.0 ± 0.5
Wiench, et al. [6]	^{27}Al	3.9 ± 0.1	0.24 ± 0.05	103.8 ± 0.8
This work	^{27}Al	3.9 ± 0.1	0.25 ± 0.5	101.6 ± 0.5
This work	^{7}Li	0.040 ± 0.003	n.a	

TABLE IV. Calculated solid-state NMR parameters for ^{27}Al and ^{7}Li in LiAlPh$_4$. The first row for each nuclei are from a planewave pseudopotential Quantum Expresso calculations and the remaining are CRYSTAL14 calculations.

nucleus	Method	C$_Q$ MHz	σ (ppm)
^{27}Al	PBE QE	-0.703	422.37
	PBE 6-311	-1.04	-
	PBE POB	-0.814	-
	B3LYP 6-311	-0.874	-
	B3LYP POB	-0.647	-
^{7}Li	PBE QE	0.0374	93.35
	PBE 6-311	0.0281	-
	PBE POB	0.0188	-
	B3LYP 6-311	0.0185	-
	B3LYP POB	0.0120	-

TABLE V. Our experimental measurements of NMR parameters for LiAlPh$_4$.

Nucleus	$|C_Q|$ MHz	δ (ppm)
^{27}Al	0.82 ± 0.1	132.0 ± 0.5
^{7}Li	0.028 ± 0.002	

TABLE VI. Experimental chemical shifts and experimental and theoretical chemical shieldings for ^{13}C in LiAlPh$_4$.

	Experiment		Theory (QE)	
Atom	δ (ppm)	σ (ppm)	Atom	σ (ppm)
C1	150.5 ± 0.2	19.4 ± 0.2	C1	19.29
C2	142.9 ± 0.2	27.0 ± 0.2	C2	26.06
C3 and C4	129.2 ± 0.2	40.7 ± 0.2	C3	40.74
			C4	40.99
C5 and C6	132.4 ± 0.2	37.5 ± 0.2	C5	36.73
			C6	38.95

forces the gradients of the electric field at both nuclei to be identical in the two perpendicular directions, and thus $\eta = 0$ in the case where the largest electric-field gradients at both atoms are along the bond. In all calculations $\eta = 0$ and no tables contain a column for η. For the C$_Q$ there is about twenty percent dispersion between all techniques and all values are negative for ^{27}Al. For ^{7}Li the C$_Q$ values are quite small, all positive, and the dispersion is much greater perhaps due to the small absolute value of this NMR parameter. In the CRYSTAL calculations, the B3LYP functional gives smaller values of C$_Q$ than PBE for a given basis set and the POB basis set gives smaller values of C$_Q$ for a given functional. The QE C$_Q$ for ^{27}Al agrees best and is within fifteen percent of the PBE POB CRYSTAL calculation. The QE C$_Q$ for ^{7}Li agrees best and is within thirty percent of the PBE 6-311 CRYSTAL calculation. In comparison to values computed for LiAlH$_4$, the theoretical chemical shifts in LiAlPh$_4$ are lesser for the ^{27}Al nuclei and greater for the ^{7}Li nuclei.

The experimental NMR parameters for ^{27}Al and ^{7}Li within LiAlPh$_4$ are shown in Table V. Again, the difference with theory is in the sign of C$_Q$ for ^{27}Al, which is not determined experimentally. There is rather good agreement between the magnitude of the average of the theoretical values and the experimental C$_Q$ values for both nuclei.

The calculated chemical shielding for ^{27}Al in LiAlPh$_4$ is reduced by about 35 ppm relative to that of LiAlH$_4$. The experimental chemical shift increases by 30.4 ppm which is in quite good agreement. We believe that the reduced chemical shielding can be primarily attributed to an electron-withdrawing effect of the aromatic phenyl groups on the central Al atom.

The unique carbon atoms in LiAlPh$_4$ are labeled clockwise around a phenyl ring on the left side of Fig. 3. There is a lithium atom above C6 and C1. C1 is bonded to the Al atom. Because of the S$_4$ symmetry of this cluster, the numbering appears counterclockwise from the perspective of the other lithium atom. The experimental and calculated chemical shieldings for ^{13}C in LiAlPh$_4$ are shown in Table VI. Theoretical shieldings were obtained from QE, as they cannot by calculated with CRYSTAL. The experimental data was fitted using the equation $\sigma = 169.9 - \delta$. The chemical shift decreases with distance from the Al atom, except for C6. Perhaps the reason for this discrepancy is that C6 is the carbon atom that lies closest to Li. In the PBE 6-311 optimization this internuclear distance is 2.55 Å. The C1 nucleus is only 0.09 Å more distant, but the other carbon atoms are much further away. For comparison the Al-C1 distance is 2.01 Å. Note that ^{13}C is a spin-$\frac{1}{2}$ nucleus; thus, its quadrupole moment is zero and there is no associated quadrupolar interaction. The total range of calculated chemical shieldings is 21.7 ppm while the total range of experimental chemical shifts is 21.3 ppm. This highlights the advantage of being able to compare more than one shift in a single calculation, i.e., the linear scaling is now feasible without doing an additional reference calculation.
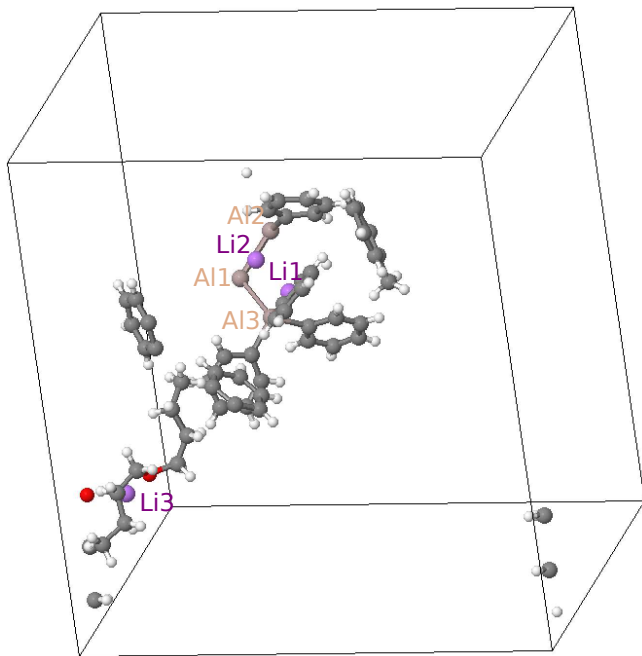
FIG. 4. The asymmetric unit cell of $[\text{Li}(\text{Bu}_2\text{O})_3][\text{Li}_4\text{Al}_5\text{Ph}_{12}]$.

As J-coupling calculations are not yet available for periodic crystals, we performed gas-phase Gaussian09 calculations on an isolated $\text{Li}_2\text{AlPh}_4+$ ion at the atomic positions given by the CRYSTAL PBE LiAlPh_4 calculation. We used the nmr = spinspin and the 6-311G+(d,p) basis set and obtained 78 Hz for the Al-C1 J-coupling constant (where C1 is as labeled in Fig. 3). This is in good agreement with the J-coupling of 94 ± 2 Hz determined from the ^{13}C NMR spectrum at 2.35 T.

C. $[\text{Li}(\text{Bu}_2\text{O})_3][\text{Li}_4\text{Al}_5\text{Ph}_{12}]$

We were unable to isolate a sufficient quantity of crystalline $[\text{Li}(\text{Bu}_2\text{O})_3][\text{Li}_4\text{Al}_5\text{Ph}_{12}]$ for reliably reproducible NMR measurements. Additionally, due to difficulties with convergence in CRYSTAL and limitations in our computational resources, we are only able report parameters obtained with QE. However, we expect the good agreement between experiment and both theoretical methods that was seen with the other Al compounds to carry over to this larger one as well.

Table VII contains the computed quadrupolar coupling constants, asymmetry parameters, and chemical shielding for Al and Li atoms in $[\text{Li}(\text{Bu}_2\text{O})_3][\text{Li}_4\text{Al}_5\text{Ph}_{12}]$. This cluster contains multiple Al and Li environments, as determined by symmetry. Three of the five Li atoms are symmetrically independent, and are numbered in the asymmetric unit cell in Fig. 4.

Al1, the central aluminum of the $[\text{Li}_4\text{Al}_5\text{Ph}_{12}]^-$ cluster anion, and is bound to four AlPh_3 moieties in a local tetrahedral environment. The four AlPh_3 groups are di-

TABLE VII. Calculated solid-state NMR parameters for ^{27}Al and ^7Li in $(\text{Bu}_2\text{O})_3\text{Li}_5\text{Al}_5\text{Ph}_{12}$. The first row for each nuclei are from a planewave pseudopotential Quantum Expresso calculations and the remaining are CRYSTAL14 calculations.

nucleus	Method	C_Q MHz	η	σ (ppm)
$^{27}\text{Al1}$	PBE QE	-0.081	0.589	557.56
$^{27}\text{Al2}$	PBE QE	1.84	0.419	416.56
$^{27}\text{Al3}$	PBE QE	2.78	0.147	413.18
$^7\text{Li1}$	PBE QE	0.072	0.408	90.23
$^7\text{Li2}$	PBE QE	0.089	0.708	90.08
$^7\text{Li3}$	PBE QE	-0.432	0.666	92.00

vided into two symmetry inequivalent groups, and therefore the aluminum atoms in these units are labeled Al2 and Al3. Similarly, there are two additional Li cations in the full translational unit cell related to Li1 and Li2 by symmetry.

The difference in the chemical shielding between Al1 and Al2 is 141 ppm and between Al1 and Al3 the difference is 143.38 ppm. The computed chemical shielding for all three aluminum nuclei are very far from metallic aluminum, which appears at approximately 1640 ppm.

VI. CONCLUSION

A large number of low oxidation state aluminum clusters have been synthesized to date, and evolving synthetic techniques hold the promise of isolating more [1]. Clusters that have been isolated in the solid state thus far typically exhibit high molecular symmetry, and this study lays the groundwork for using NMR to understand them. In principle, the $[\text{AlH}_4]^-$ anion is simpler and more symmetric than $[\text{AlPh}_4]^-$, which in turn is simpler and more symmetric than $[\text{Li}_4\text{Al}_5\text{Ph}_{12}]^-$. Yet, the Li and Al η NMR parameters for LiAlPh_4 are both zero because of the high crystal symmetry, whereas they are not for the other two.

The calculations performed with QE and CRYSTAL are in principal the same, despite the difference in the form of the basis sets. All calculations assumed frozen core orbitals and had large, what we expect to be triple-ζ or better, valence basis sets. Computationally, planewaves-pseudopotential and all-electron-Gaussian calcuations are very different, yet by and large, we found agreement between the two methods.

We found generally good agreement between experiment and theory, although for quantities that are large in magnitude, there is approximately a ten percent disagreement, which is also present between theoretical methods. We expect this will hold for the $[\text{Li}(\text{Bu}_2\text{O})_3][\text{Li}_4\text{Al}_5\text{Ph}_{12}]$ cluster as well, where experimental measurements and CRYSTAL calculations could not be obtained. The biggest differences in theoretical values, much more than a factor of two, are for the Li η values. Only for this case are the corresponding experimental values difficult

to determine due to the small Li nuclear quadrupole moment. One theoretical method does not give clearly better agreement with experiment than another, and, contrary to our expectation, B3LYP results are not in better agreement with experiment. The two Gaussian basis sets differ significantly in number of contracted basis functions for Al, but the larger 6-311 basis does not uniformly agree better with experiment. In fact, taking an average of the theoretical results might be the best approach, for now, to unraveling metalloid chemistry.

[1] H. Schnöckel, Chem. Rev. **110**, 4125 (2010), pMID: 20540559.

[2] J. Vollet, J. R. Hartig, and H. Schnöckel, Angew. Chem. Internat. **43**, 3816 (2004).

[3] D. Bono, J. Hartig, M. Huber, H. Schnöckel, and L. J. de Jongh, J. Cluster Science **18**, 319 (2007).

[4] J. Zuckerman and A. Hagen, *Inorganic Reactions and Methods, The Formation of Bonds to C, Si, Ge, Sn, Pb*, Inorganic Reactions and Methods No. pt. 3 (Wiley, 2009).

[5] B. Hauback, H. Brinks, and H. Fjellvg, J. Alloys Compd. **346**, 184 (2002).

[6] J. Wiench, V. Balema, V. Pecharsky, and M. Pruski, J. Solid State Chem. **177**, 648 (2004).

[7] L. Kellberg, H. Bildse, and H. J. Jakobsen, J. Chem. Soc., Chem. Commun. **19**, 1294 (1990).

[8] F. Mauri, B. G. Pfrommer, and S. G. Louie, Phys. Rev. Lett. **77**, 5300 (1996).

[9] D. Ceresoli, N. Marzari, M. G. Lopez, and T. Thonhauser, Phys. Rev. B **81**, 184424 (2010).

[10] P. Giannozzi, S. Baroni, N. Bonini, M. Calandra, R. Car, C. Cavazzoni, D. Ceresoli, G. L. Chiarotti, M. Cococcioni, I. Dabo, A. D. Corso, S. de Gironcoli, S. Fabris, G. Fratesi, R. Gebauer, U. Gerstmann, C. Gougoussis, A. Kokalj, M. Lazzeri, L. Martin-Samos, N. Marzari, F. Mauri, R. Mazzarello, S. Paolini, A. Pasquarello, L. Paulatto, C. Sbraccia, S. Scandolo, G. Sclauzero, A. P. Seitsonen, A. Smogunov, P. Umari, and R. M. Wentzcovitch, J. Phys. Condens. Matter **21**, 395502 (2009).

[11] N. Stone, At. Data and Nucl. Data Tables **90**, 75 (2005).

[12] R. Dovesi, R. Orlando, A. Erba, C. M. Zicovich-Wilson, B. Civalleri, S. Casassa, L. Maschio, M. Ferrabone, M. De La Pierre, P. D'Arco, Y. Noël, M. Causà, M. Rérat, and B. Kirtman, Int. J. Quant. Chem. **114**, 1287 (2014).

[13] J. P. Perdew, K. Burke, and M. Ernzerhof, Phys. Rev. Lett. **77**, 3865 (1996).

[14] C. Bonhomme, C. Gervais, F. Babonneau, C. Coelho, F. Pourpoint, T. Azas, S. E. Ashbrook, J. M. Griffin, J. R. Yates, F. Mauri, and C. J. Pickard, Chem. Rev. **112**, 5733 (2012), pMID: 23113537.

[15] R. Orlando, M. De La Pierre, C. M. Zicovich-Wilson, A. Erba, and R. Dovesi, J. Chem. Phys. **141**, 104108 (2014), https://doi.org/10.1063/1.4895113.

[16] K. Lejaeghere, G. Bihlmayer, T. Björkman, P. Blaha, S. Blügel, V. Blum, D. Caliste, I. E. Castelli, S. J. Clark, A. Dal Corso, S. de Gironcoli, T. Deutsch, J. K. Dewhurst, I. Di Marco, C. Draxl, M. Dułak, O. Eriksson, J. A. Flores-Livas, K. F. Garrity, L. Genovese, P. Giannozzi, M. Giantomassi, S. Goedecker, X. Gonze, O. Grånäs, E. K. U. Gross, A. Gulans, F. Gygi, D. R. Hamann, P. J. Hasnip, N. A. W. Holzwarth, D. Iuşan, D. B. Jochym, F. Jollet, D. Jones, G. Kresse, K. Koepernik, E. Küçükbenli, Y. O. Kvashnin, I. L. M. Locht, S. Lubeck, M. Marsman, N. Marzari, U. Nitzsche, L. Nordström, T. Ozaki, L. Paulatto, C. J. Pickard, W. Poelmans, M. I. J. Probert, K. Refson, M. Richter, G.-M. Rignanese, S. Saha, M. Scheffler, M. Schlipf, K. Schwarz, S. Sharma, F. Tavazza, P. Thunström, A. Tkatchenko, M. Torrent, D. Vanderbilt, M. J. van Setten, V. Van Speybroeck, J. M. Wills, J. R. Yates, G.-X. Zhang, and S. Cottenier, Science **351** (2016), 10.1126/science.aad3000.

[17] A. D. Becke, J. Chem. Phys. **98**, 5648 (1993), https://doi.org/10.1063/1.464913.

[18] M. J. Frisch, G. W. Trucks, H. B. Schlegel, G. E. Scuseria, M. A. Robb, J. R. Cheeseman, G. Scalmani, V. Barone, B. Mennucci, G. A. Petersson, H. Nakatsuji, M. Caricato, X. Li, H. P. Hratchian, A. F. Izmaylov, J. Bloino, G. Zheng, J. L. Sonnenberg, M. Hada, M. Ehara, K. Toyota, R. Fukuda, J. Hasegawa, M. Ishida, T. Nakajima, Y. Honda, O. Kitao, H. Nakai, T. Vreven, J. A. Montgomery, Jr., J. E. Peralta, F. Ogliaro, M. Bearpark, J. J. Heyd, E. Brothers, K. N. Kudin, V. N. Staroverov, R. Kobayashi, J. Normand, K. Raghavachari, A. Rendell, J. C. Burant, S. S. Iyengar, J. Tomasi, M. Cossi, N. Rega, J. M. Millam, M. Klene, J. E. Knox, J. B. Cross, V. Bakken, C. Adamo, J. Jaramillo, R. Gomperts, R. E. Stratmann, O. Yazyev, A. J. Austin, R. Cammi, C. Pomelli, J. W. Ochterski, R. L. Martin, K. Morokuma, V. G. Zakrzewski, G. A. Voth, P. Salvador, J. J. Dannenberg, S. Dapprich, A. D. Daniels, Ö. Farkas, J. B. Foresman, J. V. Ortiz, J. Cioslowski, and D. J. Fox, "Gaussian 09 Revision A.1," Gaussian Inc. Wallingford CT 2009.

[19] https://sites.google.com/site/dceresoli/pseudopotentials.

[20] R. Krishnan, J. S. Binkley, R. Seeger, and J. A. Pople, J. Chem. Phys. **72**, 650 (1980), https://doi.org/10.1063/1.438955.

[21] J. Heyd, J. E. Peralta, G. E. Scuseria, and R. L. Martin, J. Chem. Phys. **123**, 174101 (2005), https://doi.org/10.1063/1.2085170.

[22] M. F. Peintinger, D. V. Oliveira, and T. Bredow, J. Comp. Chem. **34**, 451 (2013), https://onlinelibrary.wiley.com/doi/pdf/10.1002/jcc.23153.

[23] M. Bak, J. T. Rasmussen, and N. C. Nielsen, J. Magn. Reson. **147**, 296 (2000).